APJ, SUBMITTED: 16TH AUGUST 2004
Preprint typeset using LaTeX style emulateapj v. 11/12/01

GEMS: IN WHAT TYPE OF GALAXIES DO MOST STARS FORM AT $Z \sim 0.7$?

C. WOLF[1], E. F. BELL[2], D. H. MCINTOSH[6], H.-W. RIX[2], M. BARDEN[2], S. V. W. BECKWITH[3,4], A. BORCH[2], J. A. R. CALDWELL[3], B. HÄUSSLER[2], C. HEYMANS[2], K. JAHNKE[5], S. JOGEE[3], K. MEISENHEIMER[2], C. Y. PENG[7], S. F. SÁNCHEZ[5], R. S. SOMERVILLE[3], L. WISOTZKI[5]

[1] Department of Physics, Denys Wilkinson Bldg., University of Oxford, Keble Road, Oxford, OX1 3RH, U.K.
[2] Max-Planck-Institut für Astronomie, Königstuhl 17, D-69117 Heidelberg, Germany
[3] Space Telescope Science Institute, 3700 San Martin Drive, Baltimore, MD 21218, U.S.A.
[4] Johns Hopkins University, Charles and 4th Street, Baltimore, MD 21218, U.S.A.
[5] Astrophysikalisches Institut Potsdam, An der Sternwarte 16, D-14482 Potsdam, Germany
[6] Dept. of Astronomy, University of Massachusetts, 710 North Pleasant Street, Amherst, MA 01003, U.S.A.
[7] Steward Observatory, University of Arizona, 933 North Cherry Avenue, Tucson, AZ 85721, U.S.A.

APJ, SUBMITTED: *16th August 2004*

ABSTRACT

We combine high-resolution images from GEMS with redshifts and spectral energy distributions from COMBO-17 to explore the morphological types of galaxies that contribute most to the UV luminosity density at $z \sim 0.7$. We analysed restframe 280 nm and V-band luminosities of 1483 galaxies in the redshift range $0.65 < z < 0.75$, along with visual morphological classifications from F850LP images (approximately rest-frame V-band) taken with HST/ACS on the Extended Chandra Deep Field South. We derive UV luminosity functions and j_{280} luminosity densities for spheroids (E-S0), spirals (Sa-Sd), irregulars and clearly interacting galaxies (Pec-Int) suggestive of ongoing major mergers. We check the reliability of GEMS morphologies against the deeper GOODS images and quantify an incompleteness of the GEMS merger identification at the faint end. We derive the fractions of the global UV luminosity density j_{280} originating from the galaxy types, and find that Sa-Sd spirals and Irregulars dominate with about 40% share each. Interacting and merging galaxies account for roughly 20% of j_{280}, while the contribution of early types is negligible. These results imply that the strong decline in the UV luminosity density of the Universe observed from $z \sim 1$ until today is primarily due to decreasing star formation rates in normal spirals, accompanied by the migration of high star formation rates in irregulars to systems of progressively lower mass and luminosity. Our analysis shows that any decline in major merger rates can not be an important factor in the waning of the cosmic SFR. This conclusion holds, unless major mergers were on average extremely dust-obscured, and the decline in obscured cosmic star formation was even stronger than the already impressive decline implied by the uncorrected UV luminosity density.

Subject headings: Surveys – Galaxies: evolution – Galaxies: general – Galaxies: luminosity function – Galaxies: morphology

1. INTRODUCTION

It is well established that the UV luminosity density integrated over the galaxy population in the Universe drops from $z \gtrsim 1$ to the present day (Madau et al. 1996; Lilly et al. 1996; Cowie et al. 1996; Madau et al. 1998). This is one of the more impressive trends of galaxy evolution, amounting to a factor of three to six decline between $z = 0.7$ and $z = 0$ at λ_{rest} = 280 nm (Lilly et al. 1996; Cowie et al. 1996; Wilson et al. 2002; Wolf et al. 2003) [1]. Because UV light is emitted by young, massive stars, this decline is generally linked to a dramatic decline in the global cosmic star formation rate (SFR), suggesting that $> 50\%$ of all stars formed prior to $z = 1$. Despite the fact that most of the UV photons are absorbed by dust (Wang & Heckman 1996), observations of less dust-sensitive SFR indicators support this interpretation (Flores et al. 1999; Haarsma et al. 2000; Yan et al. 1999), although they do not reach as far down the luminosity function. Indeed, there is evidence that star formation is more obscured on average at $z \sim 1$ than today (Adelberger & Steidel 2000), implying an even more rapid decline in star formation rate than the uncorrected UV luminosity density would indicate.

The physics that drives this decline remains unclear. Observations of damped Lyman-α systems and local HI surveys indicate that the cosmic density of cold neutral gas also declines dramatically from $z \sim 1$ to the present (e.g. Storrie-Lombardi, McMahon, & Irwin 1996), and this is presumably directly connected with the decline in cosmic star formation rate. Some of the decline in cold gas is simply because a significant fraction of the available baryons become locked up in long-lived stars (Pei, Fall, & Hauser 1999). The hierarchical formation of massive structures at $z \lesssim 2$ also leads to a larger fraction of gas being in a shocked warm/hot phase, with long cooling times (e.g. Cen & Ostriker 1999). If the efficiency of star formation is linked to the surface density of gaseous disks, as suggested by local observations (Kennicutt 1998), and if gas disks are denser at high redshift, this would make the decline in cosmic star formation rate even steeper (Somerville, Primack & Faber 2001). In addition, if galaxy interactions trigger efficient bursts of star formation (e.g. Sanders & Mirabel 1996), then a decline in the merger rate will also contribute to a more rapid decline in star formation over this period. Observations have shown that the merger rate has probably dropped significantly since $z \sim 1$, although the degree of the evolution is still subject to debate (Le Fèvre et al. 2000; Carlberg et al. 2000; Patton et al. 2002; Conselice et al. 2003).

The characteristic rise and decline of the cosmic star formation rate is a generic prediction of cosmological simulations of galaxy formation in the Cold Dark Matter framework (Baugh et al. 1998; Somerville et al. 2001; Nagamine et al. 2000; Springel & Hernquist 2003; Hernquist & Springel 2003). But the location of the SFR maximum and the rate of the decline on either side depend on the input physics, especially the treatment

[1] In this paper we assume $(\Omega_m, \Omega_\Lambda) = (0.3, 0.7)$ and $H_0 = h \times$ 100 km/sec with $h = 1$

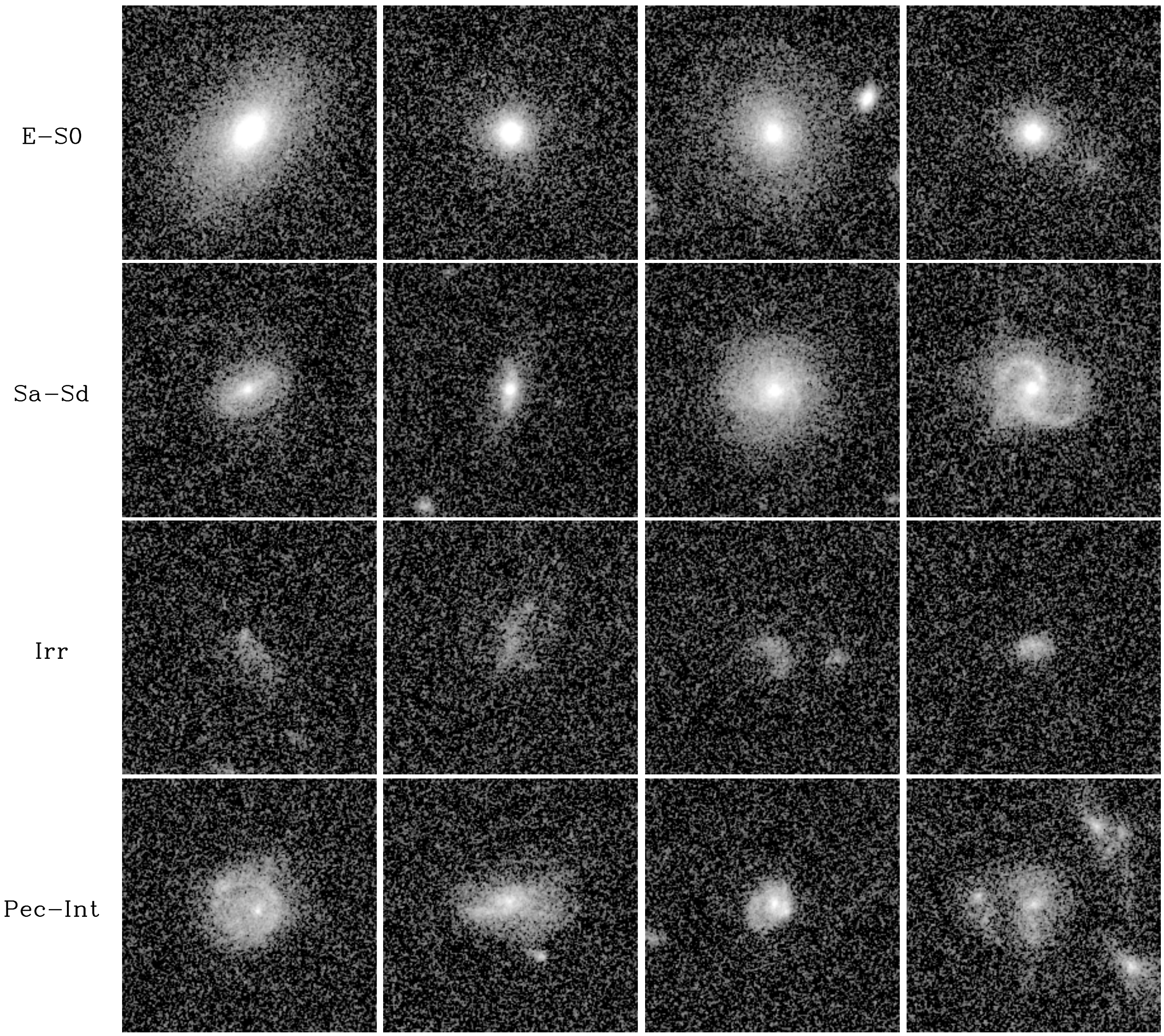

FIG. 1.— Morphological classification: HST/ACS F850LP images of the four types with four examples each. Panels measure $6'' \times 6''$. *From top row to bottom row:* E-S0 — Sa-Sd — Irr — Pec-Int.

of star formation and feedback. Hence, observational tests of star formation in different types of galaxies are very interesting for discriminating between different models.

In this paper, we present progress towards pinning down the underlying physics responsible for the decline in the cosmic star formation rate: We investigate the contributions of galaxies with different morphological types to the UV luminosity density of the Universe at $z \sim 0.7$. For this investigation we combine high spatial resolution imaging with the Advanced Camera for Surveys (ACS) on the Hubble Space Telescope from the GEMS (Galaxy Evolution from Morphology and SEDs; Rix et al. 2004) survey with accurate photometric redshifts and restframe UV/optical luminosities and colors from COMBO-17 (Classifying Objects by Medium-Band Observations in 17 filters; Wolf et al. 2001; Wolf et al. 2004). In particular, we will assess the UV luminosity contribution of manifestly interacting or morphologically peculiar galaxies at $z \sim 0.7$ compared to, e.g., luminous spirals. We restrict our attention to a redshift slice at $0.65 < z < 0.75$, where the ACS F850LP band corresponds roughly to the rest-frame V-band, in order to bypass uncertainties due to morphological K-corrections and to minimize any redshift-dependent selection effects, e.g. due to cosmological surface brightness dimming. Our sample contains almost 1500 galaxies with COMBO-17 redshifts and visually classified morphological types. A more detailed study over the full redshift range probed by the GEMS sample will be presented in future work.

The restframe UV luminosity is an important tracer for star formation all the way to $z \gtrsim 6$ (e.g. Sullivan et al. 2000; Giavalisco et al. 2002; Bouwens et al. 2003; Bunker et al. 2004). Of course, a fuller understanding of how the SFR density evolves will have to incorporate complementary constraints on the bolometric luminosity of the youngest stellar population, such as Hα-, IR- or radio luminosities. In order to directly constrain the amount of dust-obscured star formation in our sample, a preliminary analysis of Spitzer 24μm data taken by the MIPS instrument team (Rieke et al. 2004, ApJS, in press) on the Chandra Deep Field South is presented in a companion paper (Bell et al. 2004, in preparation). However, the advantage of the UV analysis presented here, is that observations of rest-frame UV probe much further down the luminosity function than all other SFR indicators at $z \gtrsim 0.5$, meaning that the total UV luminosity density is relatively reliably constrained. Finally, this study will reveal which galaxies are responsible for the changing UV ionising background at $z \lesssim 1$, because galaxies with large contributions to the 280 nm luminosity density are likely to make correspondingly large contributions to the cosmic luminosity density in the ionising background at $\lambda < 91$ nm.

The structure of this paper is as follows. In Sect. 2 we describe the data sets in more detail, and in Sect. 3 our morphological classification. In Sect. 4 we discuss the distribution of UV/optical galaxy colors, present UV luminosity functions by morphological type, and assess the contribution of different types to the restframe UV luminosity density. In Sect. 5 we discuss our results in the light of previous results and theoretical predictions, summarizing in Sect. 6.

2. DATA

The COMBO-17 survey has measured accurate photometric redshifts for more than 10,000 galaxies in the Extended Chandra Deep Field South (E-CDFS, see public data set, Wolf et al. 2004). The redshifts are estimated using data from 5 broad and 12 medium bands. Detailed comparisons with spectroscopic redshifts and simulations suggest the mean error of the redshifts to be $\sigma_z/(1+z) \sim 0.02$ at $R < 23$, the brighter half of the sample. At $R < 24$, more than 90% of the galaxies have robustly estimated redshifts.

The object sample is based on deep catalogues which have been restricted to include only galaxies with reliable redshifts and hence luminosities. For this purpose a general cut of $R < 24$ was applied, where at $z = 0.7$ the R-band corresponds to a band in restframe centered on 380 nm and with 115 nm width. The COMBO-17 filters have central wavelengths ranging from 365 to 915 nm and allow us to calculate galaxy luminosities at 280 nm or V-band directly from the observed photometry with no need for extrapolated K-corrections. We estimate errors for restframe luminosities and colors in COMBO-17, based on the errors of the photometry (for details, see Wolf et al. 2004). These should not exceed 0.2 mag including systematic aperture and calibration biases in most cases.

The GEMS survey has covered almost the whole COMBO-17 area on the E-CDFS with HST/ACS observations on an area of $\sim 800\square'$ (Caldwell et al. in preparation, Rix et al. 2004). Altogether, 77 HST/ACS pointings were observed with an exposure time of one orbit each in the F606W and F850LP passbands. The central 1/5th of the area is incorporated from the first epoch of GOODS imaging (Giavalisco et al. 2004). For galaxy classification, the images are approximately surface brightness limited, at a limiting average surface brightness within the half-light radius of $z_{AB} \sim 24$ mag/$\square''$ in the F850LP passband. We also compare results from the full-depth images of GOODS to test how results from GEMS may be systematically biased by the shallower images. We also compared our classifications based on the shallow GEMS images with those obtained from the ultra-deep UDF images (Beckwith et al. 2004), but with only 22 galaxies in our sample the use of these results is very limited.

We have removed three objects (of 1486) with luminosities in excess of $M_{280} = -22$ from the sample. Their unusually high luminosities put them far off the main sample, and make them likely to be AGN with significant nuclear light contribution. One of them is a large spheroidal galaxy contained in an area covered by deep XMM observations (PI Bergeron) and identified as an X-ray source, which makes it a likely AGN candidate. The other two objects are just outside the XMM area.

The galaxy sample used here covers the redshift spikes of the galaxy distribution in the CDFS at $z = 0.67$ and $z = 0.73$ (Gilli et al. 2003; Le Fèvre et al. 2004). It was chosen because at this redshift the observed ACS F850LP band corresponds to the restframe V-band. Altogether, the sample contains 1483 galaxies and fills a comoving volume of 42375 (Mpc/h)^3. Although the slice selects the highest-density environments known in the CDFS, it contains no massive clusters. At most redshifts, the CDFS is observed to be rather underdense compared to the cosmic average. However, this is currently still the largest sample of moderately distant galaxies with redshifts and wide-field space-based data from which morphology can be determined.

3. MORPHOLOGICAL CLASSIFICATION

Morphological classification was carried out by eye on the F850LP images for the 1483 galaxies found in the GEMS area with COMBO-17 redshifts $0.65 < z < 0.75$ and R-band aperture magnitudes $R_{\rm aper} < 24$. At this redshift, F850LP corresponds approximately to the restframe V-band. Galaxies were

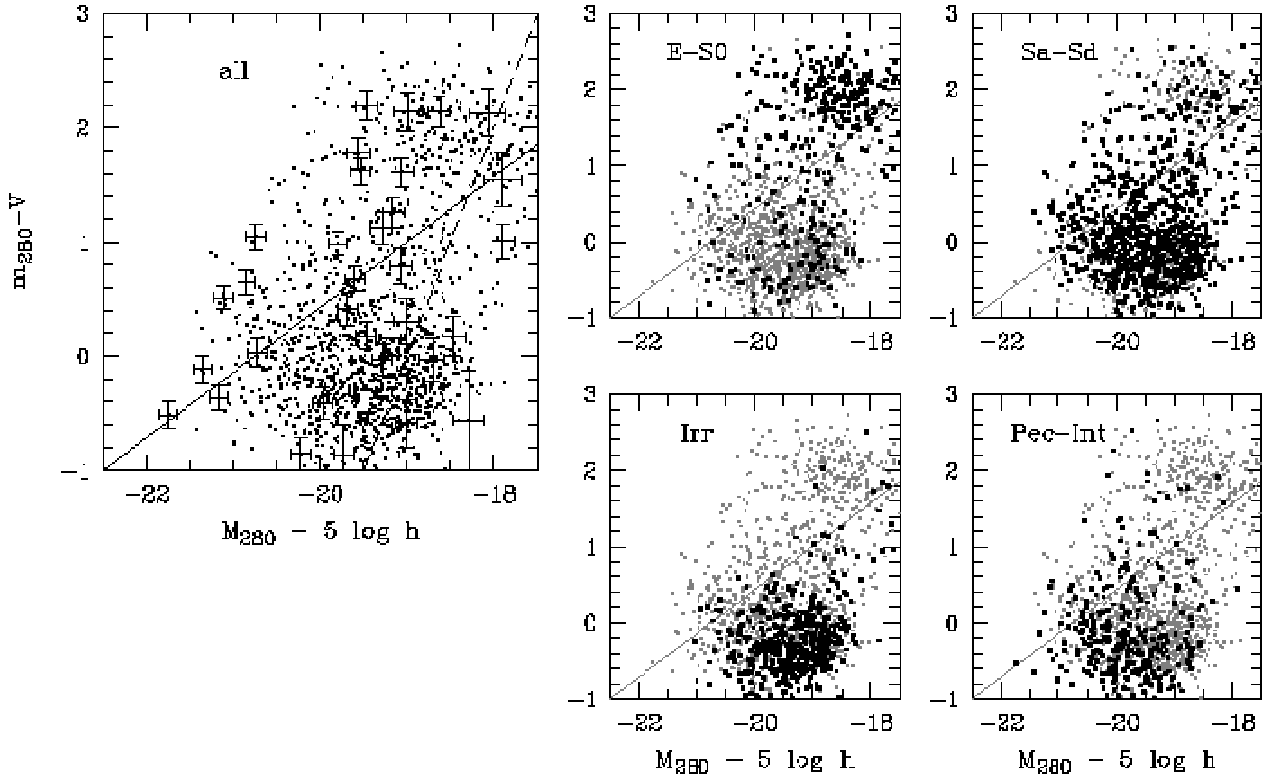

FIG. 2.— Color-magnitude diagram: *Left:* The parent sample with 1483 galaxies. A subsample has been randomly chosen to plot typical error bars including expected systematic biases. The solid line roughly represents galaxies with constant mass of $10^{10}h^{-2}M_{\odot}$, following Bell & de Jong (2001). The dashed line delineates a subsample with $> 90\%$ completeness. *Right:* Four panels showing the samples of four morphological type samples from all three classifiers combined (black dots) on top of the parent sample (grey background dots).

first sorted into a wide range of morphological classes, and later combined into a final set of four broader classes. These four are: *spheroids* (E-S0), *spirals* (Sa-Sdm), *irregulars* (Irr), and morphologically peculiar galaxies with disturbances suggestive of interaction and ongoing major mergers (Pec-Int). Objects which where barely resolved were finally included in the *irregular* bin.

We estimate the variance of this classification process by having three of the authors (EB, DM, CW) producing independent classifications: they turned out to differ most frequently in the faintest magnitude bin. Faint objects are small, thus displaying only few resolution elements, and would not clearly show their low-surface-brightness features in the noisy images. This lower discriminative power of GEMS images for faint objects leads to two effects: first, random scatter in the classification increases as the by-eye classification becomes more ill-defined. Secondly, at low signal and for small galaxies interaction features can not be discerned, which will bias the classification systematically against peculiar galaxies (Pec-Int).

We reduce the effect of random scatter onto our results by using the classifications of all three authors with a weight of 1/3rd each. When we calculate luminosity functions, e.g., we include the author-to-author variation besides Poisson noise in the error analysis. This variation dominates errors at faint levels while Poisson noise reigns at the bright end, where object numbers are small and classifications agree more often.

In order to assess systematic biases among faint galaxies, we also analyse the deeper images taken by GOODS on a five times smaller subarea. This sample is classified again by the same authors and compared against the results from the shallow GEMS images. From this comparison, we have found that all classifiers find a significantly larger fraction of faint Pec-Int galaxies in the GOODS data than in the GEMS data. The GEMS classifications of these extra Pec-Int galaxies included some early types and spirals, but were dominated by irregulars; the extra depth afforded by GOODS allowed for the recognition of faint tidal features not visible in the shallower GEMS data. This source of uncertainty is discussed further later when determining the relative contributions of different morphological types to the UV luminosity density. In constrast, we see no significant differences among other morphological types, suggesting that these are easily recognized and unbiased.

The visual classification of merging and interacting galaxies is clearly subjective, but automated classification presents also a serious challenge owing to the richness of structure in both normal spirals and interacting systems. Issues such as source extraction and segmentation, projection of very close galaxy pairs, and recognition of faint, low surface brightness tidal tails in otherwise largely relaxed systems are all important not easily modelled automatically (see Conselice 2003 and Lotz et al. 2004 for current progress on some of these issues). For this reason, we chose to explore visually-classified morphology at this time, deferring an analysis based on automated classification to a later stage. In this paper, galaxies are classified as merging or interacting if they have multiple nuclei, strongly distorted inner isophotes, or large tidal features. These visual signatures are primarily tracers of major to intermediate mass ratio (1:1 to 1:4) mergers, but may contain a tail to minor mergers with mass ratios up to 1:10.

4. RESULTS

4.1. *Colors and magnitudes*

In Fig. 2 we plot the near-UV-optical color-magnitude diagrams (CMD) for our sample split by morphological type. The CMDs of our sample display the familiar bimodality of a 'red sequence' and a 'blue cloud' of star-forming galaxies. This bimodality of galaxy colors at optical wavelengths has been observed in the local Universe (Strateva et al. 2001; Baldry et al. 2004) and out to $z \sim 1$ (Bell et al. 2004). Owing to the long wavelength base between 280 nm and the V-band ($\lambda_V/\lambda_{280} \sim 2$) and the sensitivity of the UV spectrum to ongoing star formation, galaxies span four magnitudes in rest-frame $(m_{280}-V)$ color.

The observed-frame $R < 24$ selection-cut in the parent sample translates into a UV luminosity detection limit that changes with $(m_{280}-V)$ color. As we can see in the left-hand panel of Fig. 2, increasingly red galaxies of given visual magnitude appear at decreasing M_{280} luminosities, hence the sample looks increasingly deep towards the red. The sample selection has no sharp cutoff at its faint end, because the COMBO-17 redshift completeness declines already before reaching R = 24. The completeness of the COMBO-17 galaxy catalogue depends on magnitude, redshift and galaxy type. Completeness maps have been published and discussed in great detail in Wolf et al. (2003). In Fig. 2 we also plot a rough cut for a brighter subsample that is at least 90% complete. This particular subsample is used just for the colour distributions plotted in Fig. 3.

The four right-hand panels in Fig. 2 demonstrate how galaxies of each morphological type populate the CMD. Every panel shows the full sample as grey points. Note that the incompleteness at the faint end arises from the parent sample selection in COMBO-17, restricted to galaxies with reliable photometric redshifts and luminosities.

Inspecting the CMDs more closely now, we find E-S0 galaxies mostly on the red sequence, but also some blue galaxies with smooth appearance and high light concentration. Examples of such potential blue spheroids have been seen before at medium redshift, e.g. by Menanteau et al. (2001). The CMD for spheroids looks different from more common plots of, e.g. $U-V$ vs. M_V, with the bluest spheroids being the most luminous ones in M_{280}. Plotting the same diagram over M_V would produce just a horizontally skewed version of this diagram, where then the red-sequence spheroids would be the most luminous objects instead.

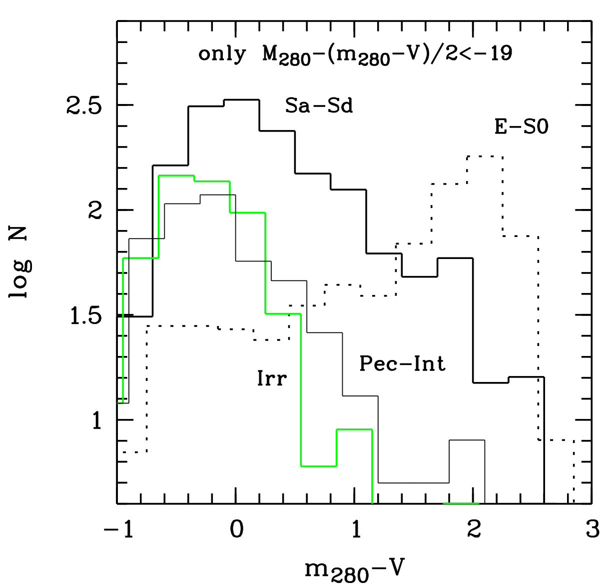

FIG. 3.— Restframe color distribution for different morphological types: Spheroids (E-S0) are predominantly red, irregulars almost uniquely very blue. Spirals and major mergers (Pec-Int) have somewhat similar distributions, with mostly blue objects and a tail to the red. Here, we only used galaxies from a brighter subsample that is at least 90% complete.

Spiral galaxies (Sa-Sd) are mostly found in the blue cloud but have a tail extending up to the red-sequence. Presumably, this tail in the color distribution is partly due to dust-reddening, in particular for edge-on spirals, but may in some cases reflect simply very low levels of star formation. Irregular galaxies have predominantly low luminosities and are almost exclusively blue, presumably because of star formation and little overall obscuration.

Our visually identified mergers (Pec-Int) have mostly blue color, but some lie in the red sequence, akin to the spirals. Most interacting galaxies on the red-sequence show clear dust lanes, but some are high-inclination objects or almost regular spheroids with left-over tidal features. The mergers tend to have luminosities above average, which is partially a result of the lacking sensitivity to classifying faint mergers in the GEMS data (see Sect. 3). However, interacting systems constitute the large majority of the rare galaxies which are simultaneously very blue and very luminous.

Overplotting a line of estimated constant stellar mass of $10^{10} h^{-2} M_\odot$ in Fig. 2 (simply based on observed colors and luminosities, following Bell & de Jong, 2001), we see irregulars predominantly below this cut at low masses. Spheroids live as expected mostly at higher mass. Major-merger candidates spread in a range of masses around the cut. Disk galaxies do the same, but with a tail to low masses.

Fig. 3 shows the number counts of the morphological samples against restframe color. Here, we use only the $> 90\%$ complete subsample to avoid any bias due to color-dependent incompleteness. Also, we are concerned about confusion of morphological types for small objects in noisy images close to the sample limit. This selection is defined by $M_{280}-(m_{280}-V)/2 < -19$. We find the color distribution of Pec-Int galaxies to be somewhat similar to that of normal spirals (and quite different from that of irregulars). Aside from the different amplitude of the two distributions, the color of the Pec-Int peak is only slightly bluer than that of spirals and the tail to the red mimics that of the spirals. The similarity may reflect the compensating effects of enhanced star formation and enhanced dust obscuration in mergers, while the merging partners originate mostly from the spiral sample.

A comparison between interacting and non-interacting galaxies in the local Universe was done by Bergvall et al. (2003), using a flux-limited sample from the ESO/Uppsala Quick Blue Survey. They found as well that the global UBV colors of interacting galaxies are quite similar to those of non-interacting galaxies, or perhaps just slightly bluer. Irregulars are very different from spirals and major mergers, being very concentrated towards the blue end of the range.

4.2. *Luminosity functions*

Near-UV luminosity functions (LF) for the four different galaxy types in the rest-frame 280 nm passband are presented in Figs. 4 and 5. In this calculation we take the explicit complete-

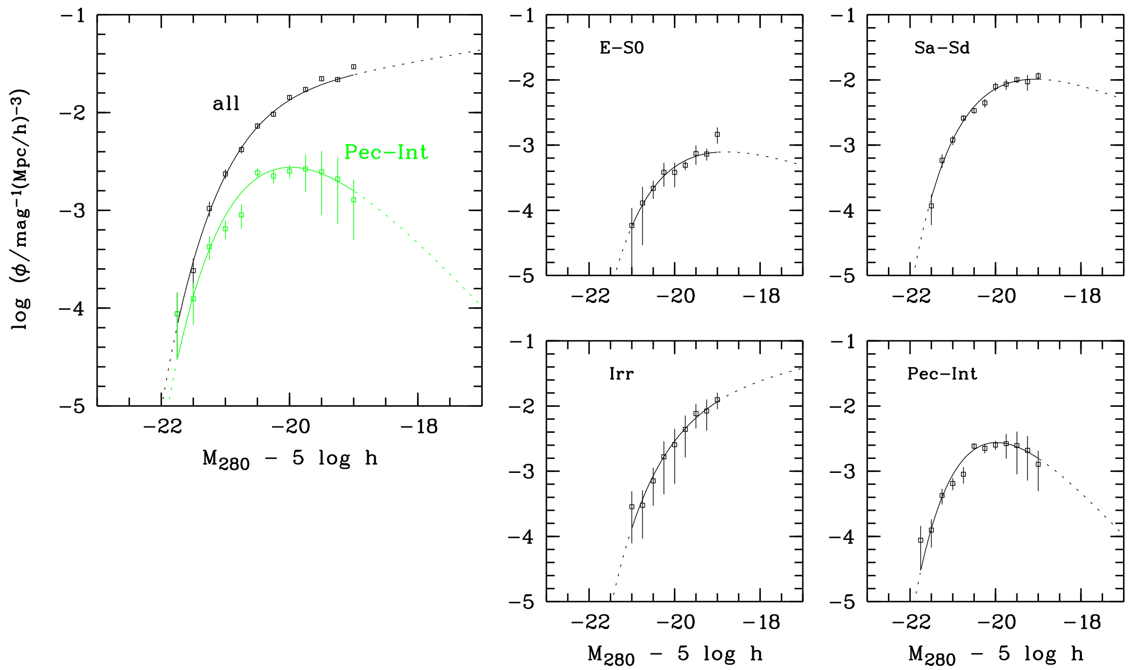

FIG. 4.— Near-UV luminosity functions from GEMS: *Left:* Parent sample with all galaxies, compared to clearly interacting galaxies. Lines are best-fitting Schechter functions. *Right:* The four morphological types, E-S0 = spheroids, Sa-Sd = spiral galaxies, Irr = irregulars, Pec-Int = clearly interacting galaxies. Error bars are from Poisson noise or author-to-author variation from their independent morphological classifications, whichever is greater.

ness maps for COMBO-17 galaxy samples into account, which depend on magnitude, redshift and restframe colour (see Wolf et al. 2003 for all equations and technical details on completeness and luminosity functions). We choose to adopt a uniform limit of $M_{280} \sim -19$ for LF calculation of this sample, essentially selected at rest-frame 380 nm. Our survey flux limit imposes the most stringent luminosity limit onto the bluest star-forming galaxies. With assumptions on faint blue spheroids we could attempt to calculate an LF for spheroids down to $M_{280} \sim -17.5$. However, since the details of faint spheroids make little difference for our conclusions, we do not pursue this possibility.

We present three sets of rest-frame UV LFs in this paper. In Fig. 4, we show the LFs of the entire GEMS sample, split by morphological type. However, comparison between classifications derived from the $5\times$ deeper GOODS data and GEMS classifications demonstrated that the GEMS data are less sensitive to lower-luminosity interactions than the GOODS data. Unfortunately, the GOODS area is only 1/5 of the GEMS area, resulting in increased uncertainties from large scale structure. We therefore address the classification bias, independent of large scale structure uncertainties, by presenting a differential deep-vs.-shallow comparison of GOODS and GEMS-derived LFs for only the subsample of 290 galaxies in the GOODS area. Altogether, we present LFs for three different samples then:

- *GEMS:* the full area with 1483 galaxies classified on shallow images, providing small statistical errors as shown in Fig. 4
- *GOODS-shallow:* the central sub-area of the GOODS field with 290 galaxies, classified on shallow GEMS-quality images
- *GOODS-deep:* the GOODS field with 290 galaxies, classified on deep GOODS images.

The LFs of GOODS-shallow and GOODS-deep are compared in Fig. 5 to assess the impact of classification on shallow images onto the LFs.

For each LF we plot V_{max} values with error bars derived from Poisson statistics or from the author-to-author variation of the space density, whichever is greater. We overplot lines of the best-fitting Schechter functions from an STY-style fit to the sample (Sandage et al. 1979) and list their parameters in Table 1. The line in the sample of all galaxies is not a fit, but the sum of the Schechter functions for the four types (see e.g. Fig. 4).

Ideally, we would like to derive the Schechter slopes independently for each of the data sets considered. However, it turns out that for some purposes the GEMS observations are not deep enough and for some the GOODS area is not wide enough to do that accurately. In the end, we combined findings from both data sets to constrain a final set of Schechter functions. Hence we discuss now both, Fig. 4 and Fig. 5, together and list all the fine-tuning steps we have applied in STY fitting here:

E/S0: The GOODS-deep sample is too small to get any useful STY fit, while the GEMS sample is large enough. Both yield unrealistic slopes of $\alpha \sim -2$. We have eliminated the galaxies belonging to last data point from the otherwise useful GEMS sample, because the data point looks strongly deviant. The CMD also shows quite a few blue spheroids around $M_{280} = -19$, but we are not sure that these barely resolved objects are correctly classified, and they may well be the most orderly looking examples of what otherwise are disks and irregulars. As a result, the STY fit for the GEMS sample yields a slope of $\alpha = -0.43 \pm 0.50$, which is perfectly plausible, albeit not well-constrained. We ended up constraining the fit of the GOODS-deep and GOODS-shallow LFs a-priori to this slope.

Sa-Sd: The Schechter function for spirals is well-constrained at least in GEMS and plausible in both samples ($\alpha_{\rm GEMS} = -0.32 \pm 0.17$ and $\alpha_{\rm GOODS-deep} = -0.52 \pm 0.41$). The LFs are determined completely independently.

Irr: In the local Universe, irregular galaxies have very steep LFs with faint characteristic luminosities, making it almost impossible to estimate any Schechter parameters robustly if the sample is not both deep and large. neither the GEMS nor the GOODS sample yielded particularly well-constrained faint-end slopes: We find $\alpha = -0.92 \pm 0.35$ from GEMS and $\alpha = -1.83 \pm 0.40$ from GOODS-deep. Since the V_{max} data points do not differ much and do not suggest a completely different LF, we ended up using the weighted mean of the two values, i.e. $\alpha_{\rm Irr} = -1.31 \pm 0.20$, for all Irr-LFs.

Pec-Int: The slope of the Pec-Int LF in GEMS is $\alpha = +0.82 \pm 0.34$, which is biased by the incompleteness of GEMS in picking up faint mergers. For the GOODS-deep STY fit, the last data point is discarded owing to its large uncertainties, yeilding a faint-end slope $\alpha = -0.15 \pm 0.50$. The increase of Pec-Int galaxies in GOODS-deep requires a corresponding decrease in other classes, because total galaxy number is conserved. The decrease is most pronounced among the irregular galaxies.

Altogether, it appears that visual classification of GEMS images biases against faint Pec-Int galaxies. Other galaxy types are easily recognized and may be randomly confused at very low S/N, but are probably unbiased. The slopes of their Schechter functions are broadly consistent with the vast literature body of local values for blue bands. The LF of spheroids in particular is consistent with the recent *B*-band results by Cross et al. (2004), who find a slope of $\alpha = -0.53 \pm 0.17$.

Comparing the GOODS-shallow LF from Fig. 5 with the GEMS LF in Fig. 4 demonstrates the effect of cosmic variance in such small fields. In the small GOODS field we see a 2-fold increase in the space density of spheroids, which probably reflects the presence of several known galaxy concentrations at $z \sim 0.7$ in the central GOODS field. In contrast, we find slightly decreased abundances of spirals and Pec-Int's.

4.3. *UV luminosity density*

Our data can directly address which galaxies are responsible for producing most of the ultraviolet luminosity at redshift $z \sim 0.7$, depending on their luminosity and their morphological type. We first determine how the contribution to the integrated UV light depends on galaxy luminosity using the Schechter fits across a wide range of magnitudes. Here, we define

$$f_{\rm mag}(M) = \frac{\int_{M-0.25}^{M+0.25} L(M)\phi(M)dM}{\int_{-\infty}^{+\infty} L(M)\phi(M)dM} \ . \quad (1)$$

The bottom panels of Fig. 6 show this fraction $f_{\rm mag}$ as derived from the LFs of GEMS and GOODS-deep, respectively. The two curves are basically indistinguishable as are the two LFs for the total galaxy sample themselves because the different classifications have only changed type labels but not the overall luminosity of the sample. While galaxies with $M_{280} \sim -20$ make the strongest contribution to j_{280}, the bulk of the UV light is emitted in the luminosity range $[-21, -18]$. Our observed galaxy sample itself provides 66% of the total UV luminosity density integrated from $-\infty$ to $+\infty$, which is $(4.70 \pm 1.17) \times 10^{12}$ W/Hz.

We can now estimate what fraction of the UV light stems from which types of galaxies. These numbers depend on the depth to which we integrate due to the different Schechter parameters of the different galaxy types. However, as long as we integrate over the bulk of the light contribution (< -18) the results should not depend very much on the depth considered. Since faint galaxies do not contribute much to the luminosity density in the Universe, the numbers converge quickly regardless of the details of LF extrapolation to very faint magnitudes. The luminosity densities and their fractions by type are here defined in dependence of the limiting depth $M_{\rm lim}$ by

$$j_{\rm type}(M_{\rm lim}) = \int_{-\infty}^{M_{\rm lim}} L(M)\phi_{\rm type}(M)dM \quad (2)$$

and

$$f_{\rm type}(M_{\rm lim}) = \frac{j_{\rm type}(M_{\rm lim})}{\sum_{\rm type} j_{\rm type}(M_{\rm lim})} \ . \quad (3)$$

The top panels in Fig. 6 show the fractions $f_{\rm type}$ derived from the Schechter fits to the luminosity function as lines, in solid style for the measured part and in dotted style where the LF is extrapolated.

Error bars show the 1-σ confidence intervals of $f_{\rm type}$ as derived from the $V_{\rm max}$ measurements for the full GEMS data set (left) and for the deeper, smaller GOODS data (right). The error bars are purely statistical, reflecting either the Poissonian limitations of the sample size or the author-to-author variation in the classification, whichever is greater. On the contrary, they neither reflect any influence from cosmic variance rendering the CDFS different from the cosmic average nor any systematic biases in the classification due to signal quality.

With respect to these two error sources, the data from GEMS and GOODS play a largely complementary role with each one having one advantage over the other: GEMS has a 5$\times$ larger field, reducing the impact of cosmic variance, whereas GOODS has substantially deeper imaging data, yielding lower classification uncertainties at faint limits.

Our sample contains 66% of the total luminosity density j_{280} of the Universe at $z \sim 0.7$. By integrating j_{280} only across the complete sample of galaxies in the GEMS sample at $M_{280} < -19$, we find more than 52 ± 3% of the light originating from spirals (author-to-author variation including Poisson noise). Irregulars and Pec-Int galaxies contribute 22% each ($\pm$5% and $\pm$2, respectively), while 3.5 ± 0.5% are from spheroids.

The GOODS sample has statistically larger error bars on all types, but less bias on faint Pec-Int's, some of which are mistaken as irregulars in GEMS. Consequently, the GOODS sample yields an increased contribution by Pec-Int's to the luminosity density of 27 ± 4%. Somewhat surprisingly this is balanced by a decreased portion arising from spirals with 45 ± 5% and from spheroids, which are lifted up to 7 ± 2%. The light fraction attributed to irregulars is largely unchanged at 21 ± 5%. Where these trends do not reflect those expected from a mere re-labelling of faint irregulars into mergers, they simply reflect the extent by which the GOODS area deviates from the cosmic average.

Fig. 6 clearly shows that the relative contributions of different galaxy types is relatively insensitive to extrapolation of the UV LFs. Spiral galaxies are still an important source of UV light, accounting for $\sim$ 40% of j_{280}, whereas E-S0 galaxies account for $\lesssim$ 5%. Owing to the steepness of the faint-end slope of irregular galaxies, their contribution to j_{280} may be as high as $\sim$ 40%. In contrast, owing to the decreasing importance of clear interactions towards fainter limits, even in the GOODS data, less than 25% of j_{280} is from clearly interacting galaxies, with a value of $\sim$ 15% in the GEMS sample alone.

We do not actually know the shape of the LF of really faint galaxies at $z = 0.7$, but we can play with an unlikely and ex-

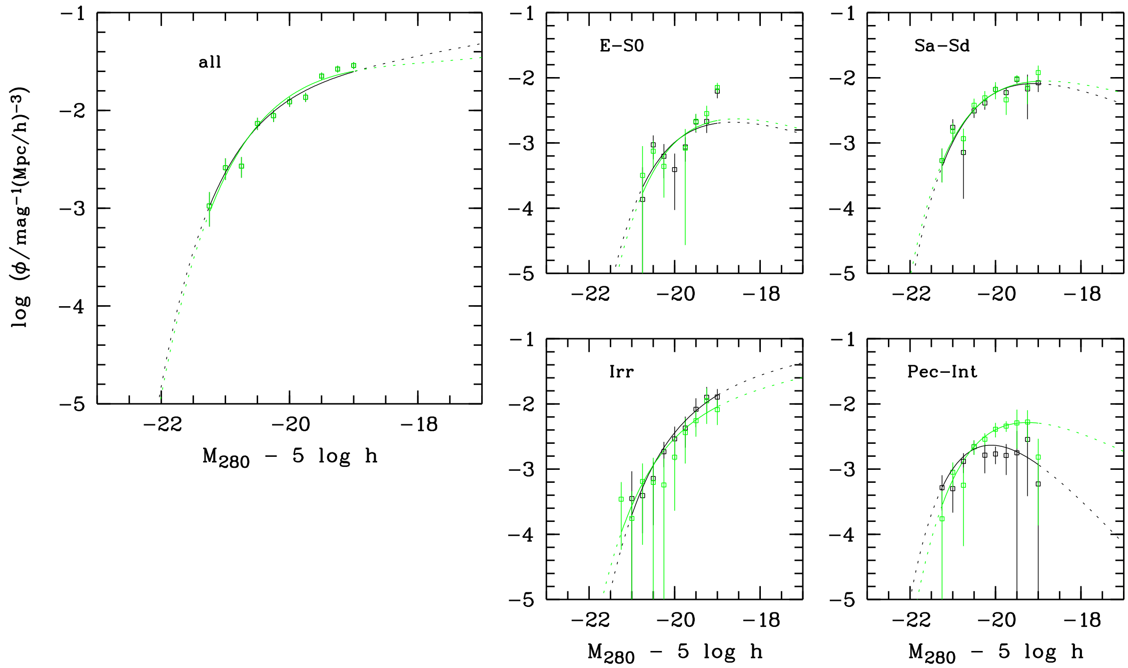

FIG. 5.— Near-UV luminosity functions from GOODS-shallow vs. GOODS-deep: The image depth influences our morphological classifications, an effect which propagates into the luminosity functions by type. Here, we compare the GEMS LF with the GOODS LF only for the 290 galaxies from the GOODS area to separate classification differences from cosmic variance. The GEMS result are shown in black and the GOODS result in grey. The major difference is that the LF of Pec-Int galaxies is increased at the faint end while irregulars are lower by a similar amount.

sample	$M^* - 5\log h$ (Vega mag)	$\phi^* \times 10^{-4}$ $(h/\mathrm{Mpc})^{-3}$	α	$j \times 10^7 L_\odot$ (h/Mpc^3)	c_{ϕ^*,L^*}
GEMS					
E-S0	−19.40±0.33	20.81± 6.01	−0.43±0.50	4.92± 1.42	−0.949
Sa-Sd	−19.49±0.11	285.93± 45.45	−0.32±0.17	74.28±11.81	−0.779
Irr	−19.33±0.17	239.70±132.52	−1.31±0.20	78.53±43.41	−1.686
Pec-Int	−19.33±0.16	62.04± 19.17	0.82±0.43	26.20± 8.10	−0.162
all	−19.67±0.16	556.35± 51.87	−0.75±0.20	183.79±45.73	−0.943
GOODS					
E-S0	−19.15±0.40	62.02± 17.76	−0.43±0.50	11.65± 3.33	−1.216
Sa-Sd	−19.64±0.31	222.27± 61.72	−0.52±0.41	64.89±18.02	−0.799
Irr	−19.65±0.36	141.19± 89.27	−1.31±0.20	61.86±39.11	−1.417
Pec-Int	−19.43±0.37	151.17± 48.52	−0.15±0.50	39.01±12.52	−0.717
all	−19.64±0.26	558.63± 70.24	−0.75±0.20	177.41±44.96	−0.975

TABLE 1

RESULTS OF STY FITS OF THE 280 NM LUMINOSITY FUNCTIONS: LISTED ARE M^*, ϕ^* WITH ITS AUTHOR-TO-AUTHOR VARIATION, j AND THE COVARIANCE BETWEEN ϕ^* AND L^*. THE j VALUES FOR THE COMBINED SAMPLE ARE ACTUALLY SUMS OVER THE j_{type}. ALL j VALUES ARE GIVEN IN UNITS OF THE SOLAR LUMINOSITY WITHIN THE 280/40 PASSBAND, WHICH IS $M_{280} = 6.66$ IN VEGA UNITS OR 2.56×10^{10} W/HZ. ERRORS ON j ARE PROPAGATED FROM ERRORS IN ϕ^*, WHICH REFLECT AUTHOR-TO-AUTHOR VARIATION IN THE LF, BUT LF SLOPE ERRORS ARE NOT PROPAGATED INTO j ERRORS.

treme thought experiment. Presume, that *all* the faint galaxies that contribute the unobserved one third of the total UV light belong to one single morphological class, whereas the other three respective classes exist only at the observed bright magnitudes. While this scenario is completely unrealistic, it would increase the j_{280} fraction of the then dominant type above the previously stated numbers by the highest possible degree. Rotating through the four classes as sole constituents of faint galaxies, we find their absolute-maximum values $f_{\rm type,max} \approx (35\%, 65\%, 50\%, 50\%)$ for (E-S0, Sa-Sd, Irr, Pec-Int), respectively.

5. DISCUSSION

We motivated our analysis with the observation that at the present day the 280 nm luminosity density is a factor of 3–6 lower than at $z = 0.7$. This drop must reflect a strong decrease in the UV luminosity of the largest contributors at $z = 0.7$, i.e. the spirals and the faint blue irregulars. A drop in the UV luminosity of ongoing mergers is expected as well. However, our results here indicate that they account for less than a quarter of the UV light at $z \sim 0.7$ to start with. Therefore, we have shown that the evolution of such mergers (even if they had completely disappeared by $z = 0$) can not be the major driver of the overall change in the UV luminosity density and the unobscured SFR of the galaxy population. This could be the most important conclusion from our observations.

5.1. *Comparison of luminosity densities*

The HST observations in the Canada-France Redshift Survey (CFRS) fields were seminal in this field, but that study was limited by sample size and depth. In their first paper, Brinchmann et al. (CFRS1, 1998) examined the types of galaxies contributing to the B-band luminosity from $z \sim 0.9$ to $z \sim 0.3$. CFRS1 used three galaxy types, i.e. *spirals*, *ellipticals* and *irregulars* including ongoing violent mergers, and found most of the decline in j_B to be a result of the evolution of spiral galaxies, which dominate j_B at the high-z end. Brinchmann et al. found that the B-band contribution from irregulars dropped at least as much as that of the spirals, although they provided a smaller contribution to begin with.

While this is fully consistent with our observations, the B-band luminosity reflects a broad range of stellar ages and is not a pure tracer of very young stars. Our results, determined in the UV, show that irregulars plus visible mergers contribute more to j_{280} then the spirals do, once we integrate also over the faint domain. This is a natural result of irregulars being bluer on average than spirals and appearing relatively more luminous in the UV.

5.2. *Comparison of merger rates*

The rate of galaxy mergers was addressed by Le Fèvre et al. (CFRS4, 2000) using visual classification. They found a dramatic increase in galaxies with merger morphologies towards higher redshift. Their merger fraction reaches 10% at $z \sim 0.63$ and even $\sim 20\%$ at $z \sim 0.9$ given a magnitude limit of $I_{AB} = 22.5$ ($I_{Vega} \approx 22.05$). Their results reflect the merger rate at the high-luminosity end, where we have also found interacting galaxies to be quite abundant. If we also limit our sample to $I_{AB} = 22.5$, then we find a merger fraction of 14% at $z \sim 0.70$, consistent with those of CFRS4.

CFRS4 conjectured that mergers be even more abundant among galaxies of lower luminosity. Our analysis implies that this is not the case: Although recognizable mergers are very common at the highest of all UV galaxy luminosities, their LF rises less quickly than the LF of the total galaxy population. Therefore, the integrated fraction of classifiable mergers actually drops with UV luminosity.

5.3. *Comparison of merger luminosity functions*

A recent study by Xu, Sun & He (2004) report the LF of K_s-selected major mergers in the local Universe, compared to all galaxies from 2MASS observations. While the identification of mergers in restframe K-band light may be a different matter than in restframe V-band, it is worth comparing the results. They show that the K_s-band LF at $z \sim 0.04$ peaks at $M_K \approx -23$ and turns down towards lower luminosities with a Schechter slope of $\alpha = +0.3 \pm 0.56$. This is just between the two slopes we have observed and certainly consistent with either one. They convert their observations into mass functions and conclude further that mergers tend to avoid both the high-mass and the low-mass domain in the local Universe. We see intriguingly similar behavior in the ultraviolet LF at $z \sim 0.7$, though it is unclear whether or not this is caused by the various selection effects.

5.4. *Effects of dust extinction*

The impact of extinction by dust is a significant uncertainty in observational probes of the cosmic star formation rate based on restframe UV luminosity measures. This is of particular concern in this study, as dust extinction is known to depend on gas content, metallicity, geometry, and stellar age — all factors that correlate strongly with morphological type. Therefore, we can not immediately conclude that contributions of various galaxy types to the UV luminosity density reflect their relative contributions to the average cosmic SFR.

Yet, an understanding of the contribution of different galaxy types to the UV luminosity density is important, both because it is possible to reach down well below the knee of the luminosity function, and because an understanding of the UV luminosity density gives some insight into, e.g., plausible sources of ionizing UV photons. Bell et al. (in preparation) use deep 24μm data from Spitzer for galaxies in the same $0.65 < z < 0.75$ galaxy sample used in this paper to constrain the importance of obscured star formation. Owing to instrumental sensitivity, $\sim 2/3$ of the GEMS sample is undetected at 24μm, accounting for 1/2 or more of the total star formation rate at $z \sim 0.7$. They find many highly-obscured galaxies, with IR/UV $\gtrsim 10$. Yet, despite this dominant contribution from the IR, the qualitative picture is very similar: $\lesssim 40\%$, and more likely $\sim 30\%$ of the total SFR (as derived from the IR and UV luminosities combined) is in clearly interacting systems, with the rest coming primarily from spiral galaxies with small contributions from irregulars and E/S0 galaxies. Their results are fully consistent with earlier ISO results (e.g., Flores et al. 1999; Zheng et al. 2004), with the important advantages of increased sample size and sensitivity. This supports the primary conclusion of this paper: a decreasing major merger rate cannot be the sole driver of the drop in cosmic star formation rate between $z \sim 1$ and the present day.

5.5. *Expectations from hierarchical models*

Somerville, Primack, & Faber (2001, hereafter SPF) made specific predictions for the fraction of star formation arising from merging galaxies, based on semi-analytic models set in the ΛCDM paradigm. In their 'collisional starburst' model, they

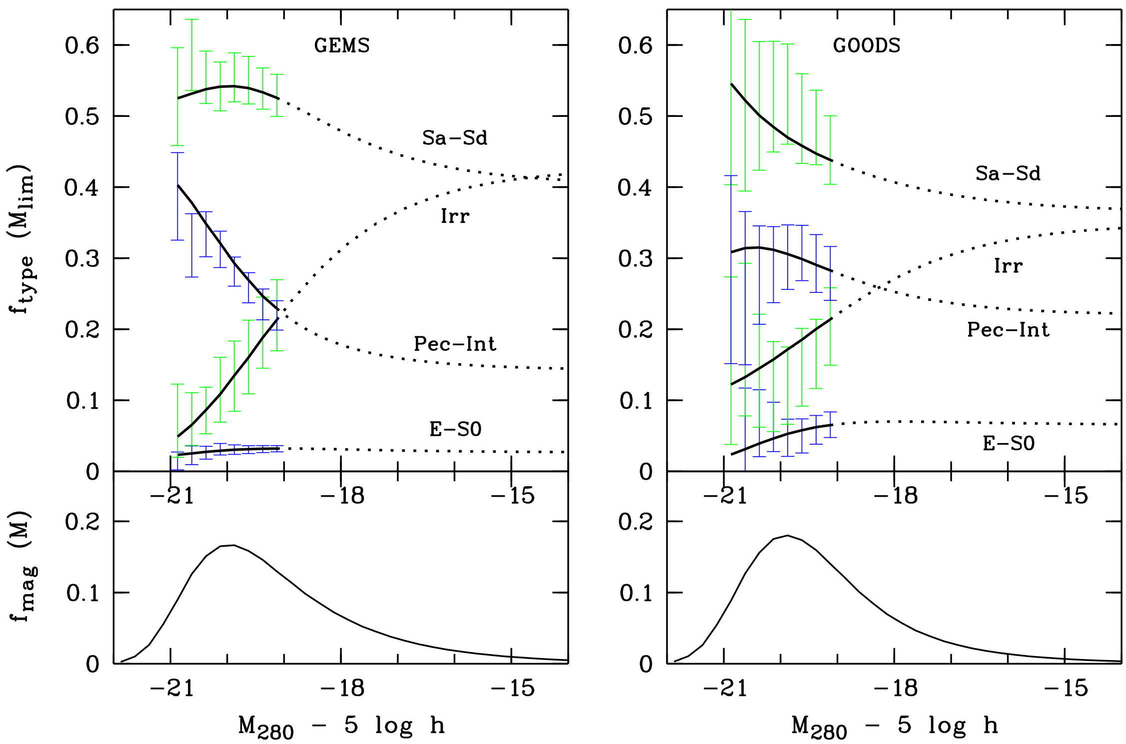

FIG. 6.— Fractional contributions to the 280 nm luminosity density from different morphological types, as derived from the wide-area GEMS mosaic (left) and the deeper, but smaller GOODS data (right): *Top panels:* Contribution $f_{\rm type}(M_{\rm lim})$ of the four galaxy types to $j_{280}(M_{\rm lim})$, depending on the depth limiting the integration. Two third of the total extrapolated light is observed by the galaxy sample. At $M_{280} \sim -15$ the total luminosity density j_{280} and its fractions have converged to an overall value. The error bars are the greater of either Poisson noise or author-to-author variation in morphological calssification. *Bottom panels:* Contribution $f_{\rm mag}(M)$ of magnitude intervals to the total integrated 280 nm luminosity density which peaks at $M_{280} \sim -20$, while most UV light comes from galaxies at $-21 < M_{280} < -18$.

distinguished between 'major' mergers (mergers with mass ratios of 4:1 or greater), which destroy any existing galactic disk and leave behind a spheroidal remnant, and 'minor' mergers (less than 4:1), which allow the disk to survive. In this model, all mergers trigger a burst of star formation, but the efficiency of the starburst increases as a function of the merger mass ratio, such that major mergers produce more efficient bursts. SPF based this function on hydrodynamic simulations of starbursts in interacting galaxies by Mihos & Hernquist (1994, 1996). In quiescent galaxies, the star formation rate was assumed to be simply proportional to the cold gas mass. The global star formation rate density produced by this model is in good agreement with dust-corrected observational estimates from $z \sim 0$–6 (SPF; Giavalisco et al. 2004), and the model also reproduces many (though not all) observational properties of low and high redshift galaxies.

The quantities of interest here may be read directly from Fig. 10 and 11 of SPF. Based on those figures, the collisional starburst model predicts that 35 % of star formation at $z = 0$ is due to bursts in galaxy interactions of all mass ratios, while only 2.5 % arises from major (4:1 or greater) mergers. At $z = 0.7$, about 50 % of the star formation is from bursts of all types, with only 3.5% arising from bursts associated with major mergers. At $z = 3$, the model predicts that 75 % of all star formation is due to collisional starbursts, while 18 % is due to major-merger bursts. This is in good agreement with the results presented here: the model predicts that a negligible fraction of the rise in the global star formation rate from $z = 0$ to $z \sim 1$ is caused by the change in the frequency of *major* mergers. A larger fraction (up to half) of the rise may be due to minor mergers. At higher redshift ($z \gtrsim 2$), the role of major mergers becomes increasingly more important.

It is worth noting that the collisional starburst model of SPF was designed to maximize the efficiency of star formation in collisional starbursts relative to the quiescent mode. It is therefore interesting that the models predict significantly *less* star formation in galaxies that are likely to be highly disturbed by mergers than our observations indicate. Any population of merging but highly dust obscured galaxies that are missing or under-represented in our UV-based census would only increase this discrepancy. This could be due to several factors. First, there is unlikely to be a simple correspondence between visually-identified clearly interacting galaxies and galaxy mergers with mass ratios lower than 4:1. Minor interactions could produce significant morphological disturbance, and owing to the greater frequency of minor interactions coupled with their longer dynamical friction timescales, it is not implausible that the identified population of clear interactions is dominated by relatively minor interactions.

Moreover, the efficiency of starbursts in galaxy interactions, particularly in minor mergers, is highly uncertain and depends on many unknown factors, such as the details of the orbit, the pre-existence of a spheroid, the inner structure of the galaxy and its dark matter halo, and the relative geometry of gas and stars in the pre-merger disk. The impact of the feedback by the strong winds that are presumably driven by the initial burst of star formation are very uncertain, and the effect of any associated active galactic nucleus triggered by the merger, even more so. The collisional starburst model of SPF may very well have assumed too high an efficiency for minor bursts. Reducing the efficiency of the lowest mass-ratio bursts would lead to a more prominent role for major mergers, because minor mergers are much more common and the cold gas supply is a limiting factor in star formation at these redshifts in the models. Furthermore, the models neglect *unbound* mergers (or fly-bys) entirely. These may play a significant role in both triggering star formation and producing moderate morphological disturbances at $z \sim 1$ (e.g. Menci et al. 2004). We will explore the effects of varying model assumptions in a future work.

Finally, it is not clear from the observation, what part of the 20% fraction in the SFR of interacting and merging galaxies was explicitly triggered by the merger event itself. The progenitor galaxies would likely have formed some amount of stars typical for disks even in the absence of the interaction.

6. SUMMARY

We have investigated the contribution of galaxies of different morphologies to the UV luminosity density of the Universe at $z \sim 0.7$. The goal was to understand in which kind of galaxies the observed decline in the UV luminosity density occured between this epoch and the present day. The experiment has shed light on the physical processes behind this drop in cosmic SFR. In particular, we have placed constraints on the fraction of the UV luminosity density arising from clearly interacting galaxies at $z \sim 0.7$.

Our analysis was based on a sample of 1483 galaxies in a thin redshift slice at $0.65 < z < 0.75$ in the COMBO-17/GEMS field encompassing the CDFS. We have used restframe luminosities at 280 nm and in the V-band from COMBO-17 together with three independent visual morphological classifications from rest-frame V-band images from the GOODS and GEMS HST/ACS surveys. The sample was selected by an observed frame $R < 24$ cut to ensure accurate photometric redshifts, restframe luminosities and colors. We differentiated between four broad morphological types: spheroid-dominated (E-S0), disk-dominated (Sa-Sd), irregular (Irr) and peculiar or clearly interacting galaxies with morphological features indicative of ongoing major mergers (Pec-Int). The difference between Irr and Pec-Int is driven primarily by a desire to identify the cause of irregular morphological appearance; galaxies with morphologies consistent with the stochastic propagation of star formation were labelled irregular, while galaxies with features indicative of strong gravitational disturbance, such as multiple nuclei or tidal tails, were labelled Pec-Int.

Comparing the morphological classifications between the shallower GEMS images and the deeper GOODS images, we have established that GEMS images do not allow for a complete identification of merging galaxies in the faintest magnitude bin we consider. This causes an artificially steep downturn in the luminosity function of mergers from the GEMS sample. Compensating for this shortcoming, the GEMS data offer the impoartant advantage of a much larger galaxy sample with properties closer to the cosmic average, compared to GOODS.

We analysed UV-optical color-magnitude diagrams, UV luminosity functions and luminosity densities j_{280} for all morphological types of galaxies. We found, that although interacting and violently merging galaxies dominate the rare group of particularly blue and very luminous objects, their restframe colors are similar to those of otherwise normal spirals.

We found that seemingly normal disk galaxies (Sa-Sd) are the largest contributors to the UV luminosity density, emitting about half of the j_{280} at $z \sim 0.7$ and $M_{280} < -19$. The observed galaxy sample contributes 66% of the total extrapolated j_{280} from the entire galaxy population. After extrapolation, spiral galaxies emit $\sim$40% of the total UV luminosity density. The second largest contribution originates from irregulars, which are predominantly faint and blue. Their steep luminosity function drives their contribution up to about 40% of the total j_{280} in the extrapolation. Most of the remaining UV light comes from interacting systems and ongoing violent mergers, while the contribution from spheroids is negligible. The exact numbers for the merger contribution depend to some extent on the completeness of identification and the precise shape of their faint LF, but is likely to be around 20%, possibly indicating a similar fraction of the global star formation rate in mergers at $z \sim 0.7$.

Taking the UV as a proxy, these 20% contribution towards the global SFR in strongly interacting galaxies are considerably greater than the ~ 3.5 % of star formation predicted to arise from 'major mergers' (4:1 or greater) by the collisional starburst model of Somerville, Primack, & Faber (2001). However, our merger sample probably includes also pairs with mass ratios up to 10:1. Furthermore, what fraction of these 20% SFR were explicitly triggered by the merger event is unclear, given that the galaxies would have formed some amount of stars even in the absence of the interaction.

The results presented here demonstrate clearly that the drop in the UV luminosity density of the Universe since $z = 1$ largely reflects decreasing star formation rates in normal spirals. In parallel, high star formation rates in faint blue irregulars are migrating to systems of progressively lower mass and luminosity. Any evolution in the major merger rate plays only a small role in the decline of unobscured star formation. They could only be relevant for driving the decline of star formation since $z = 1$, if the average extinction levels in mergers were far above the average of highly star-forming, but otherwise normal, spiral galaxies. An ongoing analysis using Spitzer/MIPS data (Bell et al., in preparation) will provide more robust estimates of the SFRs in luminous, interacting systems.

Support for the GEMS project was provided by NASA through grant number GO-9500 from the Space Telescope Science Institute, which is operated by the Association of Universities for Research in Astronomy, Inc. for NASA, under contract NAS5-26555. EFB and SFS ackowledge financial support provided through the European Community's Human Potential Program under contract HPRN-CT-2002-00316, SISCO (EFB) and HPRN-CT-2002-00305, Euro3D RTN (SFS). SJ acknowledges support from the National Aeronautics and Space Administration (NASA) under LTSA Grant NAG5-13063 issued through the Office of Space Science. DHM acknowledges support from the National Aeronautics and Space Administration (NASA) under LTSA Grant NAG5-13102 issued through the Office of Space Science. CYP acknowledges support from NASA/JPL, under the Michelson Fellowship Program. JPL is managed for NASA by the California Institute of Technology. CW is supported by a PPARC Advanced Fellowship.

REFERENCES

Adelberger, K. L., Steidel, C. C. 2000, ApJ, 544, 218
Baldry, I. K., Glazebrook, K., et al. 2004, ApJ, 600, 681
Baugh, C. M, Cole, S., Frenk, C. S., Lacey, C. S. 1998, ApJ, 498, 504
Beckwith, S. V. W. et al., 2004, in preparation
Bell, E. F., Wolf, C., et al. 2004, ApJ, 608, 752

Bell, E. F. B., de Jong, R. S. 2001, ApJ, 550, 212
Bergvall, N., Laurikainen, E., Aalto, S. 2003, A&A, 405, 31
Bouwens, R. J., Illingworth, G. D., Rosati, P., et al. 2003, ApJ, 595, 589
Brinchmann, J., Abraham, R., Schade, D., Tresse, L., et al. 1998, ApJ, 499, 112 (CFRS1)
Bunker, A. J., Stanway, E. R., Ellis, R. S., McMahon, R. G. 2004 MNRAS, in print
Carlberg, R. G., Cohen, J. G., Patton, D. R., et al. ApJ, 2000, 532, L1
Cen, R., Ostriker, J. P. 1999, ApJ, 514, 1
Conselice, C. J. 2003, ApJS, 147, 1
Conselice, C. J., Bershady, M. A., Dickinson, M., Papovich, C. 2003, AJ, 126, 1183
Cowie, L. L., Songaila, A., Hu, E. M. 1996, AJ, 112, 839
Cross, N. J. G., et al., 2004, AJ, in print, astro-ph/0407644
Flores, H., Hammer, F., Thuan, T. X., et al. 1999, ApJ, 517, 148
Giavalisco, M. 2002, ARAA, 40, 579
Giavalisco, M., Ferguson, H. C., Koekemoer, A. M., Dickinson, M., et al. 2004, ApJ, 600, L93
Gilli, R., Cimatti, A., Daddi, E., et al. 2003, ApJ, 592, 721
Haarsma, D. B., Partridge, R. B., Windhorst, R. A., Richards, E. A. 2000 ApJ, 544, 641
Hernquist, L., Springel, V. 2003, MNRAS, 341, 1253
Kennicutt, R. 1998, ApJ, 498, 181
Le Fèvre, O., Abraham, R., Lilly, S., Ellis, R., et al. 2000, MNRAS, 311, 565 (CFRS4)
Le Fèvre, O., Vettolani, G., et al. 2004, A&A, submitted
Lilly, S. J., Le Fèvre, O., Hammer, F., Crampton, D., 1996 ApJ, 460, L1
Lilly, S., Schade, D., Ellis, R., Le Fèvre, O., et al., 1998 ApJ, 500, 75 (CFRS2)
Lotz, J. M., Primack, J., Madau, P. 2004, AJ, 128, 163
Madau, P., Ferguson, H. C., et al. 1996, MNRAS, 283, 1388
Madau, P., Pozzetti, L., Dickinson, M. 1998, ApJ, 498, 106
Marzke, R. O., daCosta, L. N., Pellegrini, P. S., Willmer, C. N. A., Geller, M. J. 1998, ApJ, 503, 617
Menanteau, F., Abraham, R. G., Ellis, R. S. 2001, MNRAS, 322, 1
Menci, N., Cavaliere, A., Fontana, A., et al. 2004, ApJ, 604, 12
Mihos, J. C., Hernquist, L., ApJ 1994, 425, L13
Mihos, J. C., Hernquist, L., ApJ 1996, 464, 641
Nagamine, K., Cen, R., Ostriker, J. 2000, ApJ, 541, 25
Patton, D. R., Pritchet, C. J., Yee, H. K. C., Ellingson, E., Carlberg, R. G. 1997, ApJ, 47, 29
Patton, D. R., Pritchet, C. J., Carlberg, R. G., et al. 2002, ApJ, 565, 208
Pei, Y. C., Fall, S. M., Hauser, M. G. 1999, ApJ, 522, 604
Rix, H.-W., et al. 2004, ApJS, 152, 163
Sandage, A., Tammann, G. A., Yahil, A. 1979, ApJ, 232, 352
Sanders, D. B., Mirabel, I. F. 1996, ARAA, 34, 749
Schade, D., Lilly, S., Crampton, D., Ellis, R., et al. 1999, ApJ, 525, 31 (CFRS3)
Somerville, R.S., Primack, J. R., Faber, S. M. 2001, MNRAS, 320, 504
Springel, V. & Hernquist, L. 2003, MNRAS, 339, 312
Spergel, D. N., Verde, L., Peiris, H. V., Komatsu, E., Nolta, M. R. 2003, ApJS, 148, 175
Storrie-Lombardi, L. J., McMahon, R. G., Irwin, M. J. 1996, MNRAS, 283, 79
Strateva, I., Ivezic, Z., Knapp, G. R., Narayanan, V. K., Strauss, M. A., et al. 2001, AJ, 122, 1861
Sullivan, M., Treyer, M. A., Ellis, R. S., et al. 2000, MNRAS, 312, 442
Wang, B., Heckman, T. M. 1996, ApJ, 457, 645
Wilson, G., Cowie, L. L., Barger, A. J., Burke, D. J. 2002, AJ, 124, 1258
Wolf, C., Meisenheimer, K., Röser, H.-J. 2001, A&A, 365, 660
Wolf, C., Meisenheimer, K., Rix, H.-W., et al. 2003, A&A, 401, 73
Wolf, C., Meisenheimer, K., Kleinheinrich, M., et al. 2004, A&A, 421, 913
Xu, C. K., Sun, Y. C., He, X. T. 2004, ApJ, 603, L73
Yan, L., McCarthy, P. J., Freudling, W., Teplitz, H. I., et al. 1999, ApJ, 519, L47
Zheng, X. Z., Hammer, F., Flores, H., Assémat, F., & Pelat, D. 2004, A&A, 421, 847